

# Crystal structure of the new FeSe<sub>1-x</sub> superconductor†

Serena Margadonna,<sup>\*a</sup> Yasuhiro Takabayashi,<sup>b</sup> Martin T. McDonald,<sup>b</sup>  
 Karolina Kasperkiewicz,<sup>a</sup> Yoshikazu Mizuguchi,<sup>c</sup> Yoshihiko Takano,<sup>c</sup>  
 Andrew N. Fitch,<sup>d</sup> Emmanuelle Suard<sup>e</sup> and Kosmas Prassides<sup>\*b</sup>

Received (in Cambridge, UK) 29th July 2008, Accepted 5th September 2008

First published as an Advance Article on the web 26th September 2008

DOI: 10.1039/b813076k

The newly discovered superconductor FeSe<sub>1-x</sub> ( $x \approx 0.08$ ,  $T_c^{\text{onset}} \approx 13.5$  K at ambient pressure rising to 27 K at 1.48 GPa) exhibits a structural phase transition from tetragonal to orthorhombic below 70 K at ambient pressure—the crystal structure in the superconducting state shows remarkable similarities to that of the REFeAsO<sub>1-x</sub>F<sub>x</sub> (RE = rare earth) superconductors.

Superconductivity at the surprisingly high temperature of 55 K has been recently reported in fluorine-doped rare-earth iron oxyarsenides, REFeAsO<sub>1-x</sub>F<sub>x</sub>.<sup>1</sup> The magnitude of  $T_c$  and the apparent similarities with the high- $T_c$  cuprate superconductors—layered structural motifs of the conducting FeAs slabs and proximity to antiferromagnetic (AFM) and structural instabilities—have made these systems an intensely studied research field. The parent REFeAsO materials possess a simple tetragonal crystal structure (ZrCuSiAs-type, space group  $P4/nmm$ ) comprising layers of edge-sharing FeAs<sub>4</sub> tetrahedra interleaved with RE layers. On cooling, a structural phase transition to orthorhombic crystal symmetry (space group  $Cmma$ ) accompanied by the development of long range AFM order occurs.<sup>2</sup> The magnetic instability is suppressed upon fluorine-doping before the onset of superconductivity,<sup>3</sup> while orthorhombic symmetry survives well within the superconducting compositions.<sup>4</sup> Superconductivity can also be induced by oxygen vacancies in the REFeAsO<sub>1- $\delta$</sub>  systems.<sup>5</sup> The family of FeAs-based superconductors has now further expanded to include the related alkali-doped superconductors, A<sub>1-x</sub>A'<sub>x</sub>Fe<sub>2</sub>As<sub>2</sub> (A = alkaline earth, A' = alkali metal)<sup>6</sup> and the ternary LiFeAs phase.<sup>7</sup>

These discoveries have catalysed the search for superconducting compositions in related materials in which two-dimensional FeQ (Q = non-metal ions) slabs are also present. This search has now led to the report that superconductivity at  $\sim 8$  K occurs in the simple binary  $\alpha$ -FeSe<sub>1-x</sub> phase field for  $x = 0.12$  and 0.18.<sup>8</sup> Subsequent work has revealed resistivity onsets for the superconducting transition at temperatures as high as 13.5 K at ambient pressure.<sup>9</sup> Quite remarkably,  $T_c$  is

extremely sensitive to applied pressure and rises rapidly at a rate of 9.1 K GPa<sup>-1</sup>, reaching a value of 27 K at 1.48 GPa.<sup>9</sup>  $\alpha$ -FeSe crystallises at room temperature with the tetragonal PbO-type structure (Fig. 1) and comprises stacks of edge-sharing FeSe<sub>4</sub> tetrahedra—the FeSe packing motif is essentially identical to that of the FeAs layers in the iron oxyarsenides. On cooling, it was reported that a structural phase transition occurs near 105 K to an unidentified low-temperature structure with possible triclinic symmetry.<sup>8</sup> At present, little else is known about the electronic properties of the superconducting  $\alpha$ -FeSe<sub>1-x</sub> phases but it is reasonable to assume that Se non-stoichiometry is accompanied by the introduction of charge carriers in the 2D FeSe layers. At this stage, precise structural information on the superconducting phase of  $\alpha$ -FeSe<sub>1-x</sub> is needed and this should be the cornerstone for all subsequent understanding of the origin of superconductivity in this intriguing system.

Here we report the structural determination of the  $\alpha$ -FeSe<sub>1-x</sub> ( $x \approx 0.08$ ) binary superconductor by high-resolution synchrotron X-ray and neutron powder diffraction at temperatures between 5 and 295 K. We find that below  $T_s = 70$  K, the crystal structure becomes metrically orthorhombic (space group  $Cmma$ ), displaying an identical distortion of the FeSe slabs to that observed for the FeAs layers in the iron oxyarsenide family. The structural transition coincides with the temperature at which the temperature-dependent resistivity,  $\rho$ , shows an anomaly.

Powder samples of FeSe<sub>1-x</sub> were prepared as described before.<sup>9</sup> SQUID measurements (ZFC/FC protocols, 10 Oe) reveal the onset of bulk superconductivity below  $\sim 8$  K.

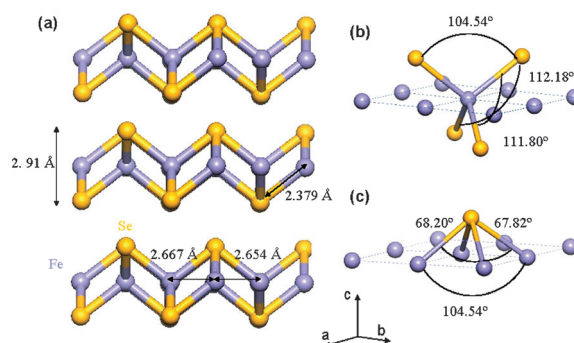


**Fig. 1** (a) Schematic diagram of the low-temperature orthorhombic crystal structure of  $\alpha$ -FeSe<sub>0.92</sub>. Fe and Se ions are depicted as blue and yellow spheres, respectively. (b), (c) Geometry of the FeSe<sub>4</sub> tetrahedra and the SeFe<sub>4</sub> pyramids with the three distinct Se–Fe–Se and Fe–Se–Fe bond angles indicated.

<sup>a</sup> School of Chemistry, University of Edinburgh, Edinburgh, UK EH9 3JJ. E-mail: serena.margadonna@ed.ac.uk

<sup>b</sup> Department of Chemistry, University of Durham, Durham, UK DH1 3LE. E-mail: K.Prassides@durham.ac.uk

<sup>c</sup> National Institute for Materials Science, 1-2-1 Sengen, Tsukuba, 305-0047, Japan

<sup>d</sup> European Synchrotron Radiation Facility, 38043 Grenoble, France

<sup>e</sup> Institut Laue Langevin, 38042 Grenoble, France

† Electronic supplementary information (ESI) available: Results of the structural refinements. See DOI: 10.1039/b813076k

Resistivity measurements by the four-probe method show the onset of superconductivity at 13.5 K with the zero-resistance state obtained at  $\sim 7.5$  K. In addition, two small humps in  $\rho(T)$  are evident near 200 and 50 K.<sup>9</sup> High-resolution synchrotron X-ray diffraction experiments were carried out on the ID31 beamline at the ESRF. The samples were sealed in 0.7 mm diameter thin-wall glass capillaries and diffraction profiles ( $\lambda = 0.40301$  Å) were collected at various temperatures between 5 and 295 K. The data were binned in the  $2\theta$  range  $1\text{--}40^\circ$  to a step of  $0.002^\circ$ . Higher statistics diffraction profiles were also recorded at 5, 100, 200 and 295 K over a longer angular range ( $2\theta = 1^\circ$  to  $50^\circ$ ). Complementary neutron powder diffraction data were collected with the high-resolution diffractometer D2b ( $\lambda = 1.5944$  Å) at the ILL. The sample (149 mg), from the same batch used for the synchrotron X-ray diffraction measurements, was loaded in a cylindrical vanadium can (diameter = 5 mm) and then placed in a standard ILL “orange” liquid helium cryostat. The instrument was operated in its high-flux mode and the data were collected in the angular range,  $2\theta = 0\text{--}164.5^\circ$  in steps of  $0.05^\circ$ . Full diffraction profiles were measured with counting times of 8 h at 5 and 295 K. The raw data were merged and normalised to standard vanadium runs using local ILL programmes. Analysis of the diffraction data was performed with the GSAS suite of Rietveld programmes.

Inspection of the synchrotron X-ray and neutron diffraction profiles of  $\alpha\text{-FeSe}_{1-x}$  at ambient temperature confirmed the primitive tetragonal (T) unit cell ( $a = 3.77376(2)$  Å,  $c = 5.52482(5)$  Å; space group  $P4/nmm$ ,  $R_{\text{wp}} = 7.87\%$  (SXRPD) and  $5.80\%$  (NPD),  $\chi^2 = 2.743$ , Fig. 1S, Table 1S†). The Se content refines to a value of  $0.91(1)$ . Additional peaks were also evident in the profiles and these could be accounted for by the presence of a minority hexagonal  $\beta\text{-FeSe}_{1-x}$  phase (space group  $P6_3/mmc$ , 22% fraction as revealed by the combined Rietveld refinements). Based on the evolution of the diffraction profiles down to 90 K the refined structure remained strictly tetragonal with both lattice constants,  $a$  and  $c$  decreasing smoothly (Fig. 2). The rate of contraction at 13.5 and  $30.0$  ppm  $\text{K}^{-1}$  for  $a$  and  $c$ , respectively, is considerably anisotropic and leads to a gradual decrease of the  $(c/a)$  ratio with decreasing temperature. However, the lattice response to further decrease in temperature below 90 K is dramatically different—the  $hkl$  ( $h, k \neq 0$ ) reflections in the diffraction profile first develop a characteristic broadening, followed by a clear splitting at  $T_s \approx 70$  K (Fig. 3) signifying a lowering in symmetry of the high-temperature tetragonal structure and the onset of a structural transition. The magnitude of the splitting increases monotonically as the sample is cooled further down to 5 K.

Combined Rietveld refinements of the synchrotron X-ray and neutron powder diffraction data of  $\alpha\text{-FeSe}_{1-x}$  at 5 K were performed successfully with the same orthorhombic (O) superstructure model (space group  $Cmma$ ,  $b > a \sim \sqrt{2}a_T$ ,  $c \approx c_T$ , where  $a_T$  and  $c_T$  are the lattice constants of the high-temperature tetragonal unit cell) employed for the low-temperature phases of  $\text{REFeAsO}_{1-x}\text{F}_x$ .<sup>2,4</sup> At 5 K, the Se content refines to  $0.92(1)$  and the refined lattice constants are  $a = 5.30781(5)$  Å,  $b = 5.33423(5)$  Å and  $c = 5.48600(5)$  Å ( $R_{\text{wp}} = 8.34\%$  (SXRPD) and  $3.77\%$  (NPD),  $\chi^2 = 2.750$ , Fig. 4, Table 1S†). The temperature evolution of the lattice constants and of the unit cell volume is shown in Fig. 2. The structural phase transition below

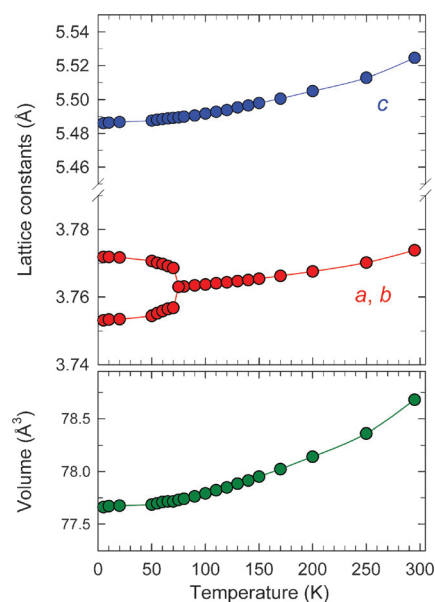


**Fig. 2** Temperature evolution of the lattice constants (top) and the unit cell volume,  $V$  (bottom) in  $\alpha\text{-FeSe}_{0.92(1)}$ . The  $a$  and  $b$  lattice constants are divided by  $\sqrt{2}$  at temperatures below the tetragonal-to-orthorhombic phase transition.

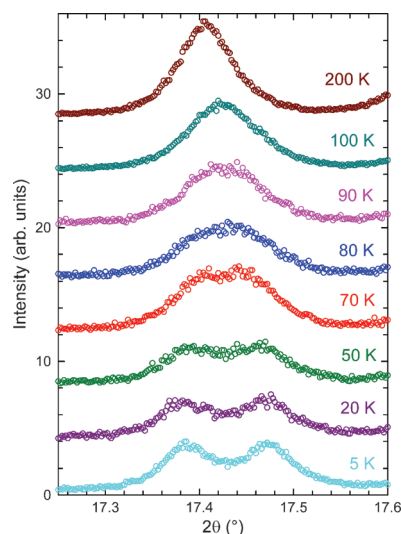


**Fig. 3** Selected region of the synchrotron X-ray diffraction profile of  $\alpha\text{-FeSe}_{0.92(1)}$  showing the temperature evolution of the  $(220)_T$  Bragg reflection which on cooling splits into a doublet  $[(040)_O, (400)_O]$  ( $\lambda = 0.40301$  Å).

70 K is accompanied by the development of orthorhombic strain in the  $ab$  basal plane—this increases continuously on cooling, approaching a value of  $s = (b - a)/(b + a) = 2.5 \times 10^{-3}$  at 5 K. However, the structural transition has no influence on the magnitude of either the interlayer  $c$  lattice constant or the unit cell volume,  $V$  as both decrease smoothly on cooling across the tetragonal–orthorhombic phase boundary. The influence of the  $T \rightarrow O$  phase transition on the local geometry of the  $\text{FeSe}_4$  tetrahedra in the  $\text{SeFeSe}$  slabs is only quite subtle (Fig. 1)—while at high  $T$ , there is a single Fe–Fe distance (at 295 K:  $2.668$  Å), below  $T_s$ , there are two symmetry inequivalent Fe–Fe distances

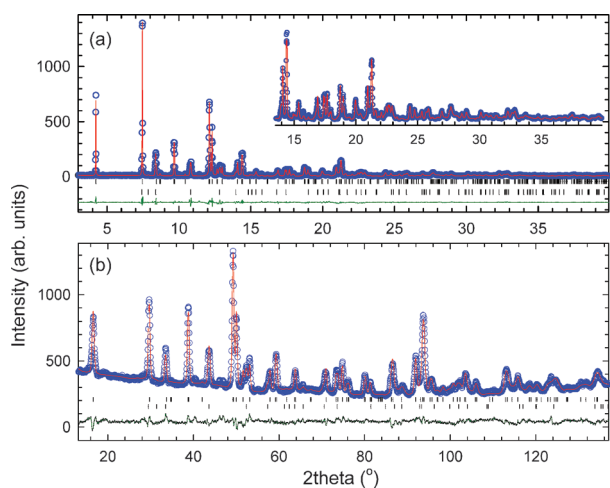


**Fig. 4** Final observed (circles) and calculated (solid lines) (a) synchrotron X-ray ( $\lambda = 0.40301 \text{ \AA}$ ) and (b) neutron ( $\lambda = 1.5944 \text{ \AA}$ ) powder diffraction profiles for the  $\alpha\text{-FeSe}_{0.92(1)}$  sample (78% fraction) at 5 K. The lower solid lines show the difference profiles and the tick marks show the reflection positions of the  $\alpha\text{-}$  (top) and  $\beta\text{-FeSe}_{1-x}$  (bottom) phases. The inset in (a) shows an expanded view of the diffraction profile at high Bragg angles.

(at 5 K: 2.667 and 2.654  $\text{\AA}$ ). Similarly, one set of the Fe–Se–Fe angles remains unaltered (at 295 K:  $104.3^\circ$ , at 5 K:  $104.5^\circ$ ), while the second set (at 295 K:  $112.1^\circ$ ) splits into two (at 5 K:  $111.8^\circ$  and  $112.2^\circ$ ). On the other hand, there is a single Fe–Se bond distance both in the tetragonal and orthorhombic phases (at 295 K: 2.389  $\text{\AA}$ , at 5 K: 2.379  $\text{\AA}$ ).

An important point arising from the present structural refinements is that the crystal structure of the superconducting state at ambient pressure in  $\alpha\text{-FeSe}_{0.92}$  is metrically orthorhombic. Moreover, there is a signature of the structural transformation in the electronic properties as  $T_s$  coincides with the observation of a hump in the temperature dependence of  $\rho(T)$ . This is reminiscent of the structural behaviour in the  $\text{SmFeAsO}_{1-x}\text{F}_x$  oxyarsenide family in which an isostructural orthorhombically distorted structure is also adopted for the superconducting compositions with F doping levels  $x \leq 0.12$ , while the  $T \rightarrow O$  phase transition is only suppressed at doping levels  $x \geq 0.15$ .<sup>4</sup> It is quite likely that an analogous suppression may occur for higher levels of Se non-stoichiometry in the present system. Certainly it is intriguing to conjecture that application of pressure may also lead to suppression of the low-temperature  $T \rightarrow O$  phase transition, thereby accounting for the remarkable enhancement of  $T_c$  upon pressurisation.

Fig. 1 shows a schematic view of the orthorhombic structure of  $\alpha\text{-FeSe}_{0.92}$ . It comprises  $\text{SeFeSe}$  slabs of  $\sim 2.91 \text{ \AA}$  thickness made of edge-sharing distorted  $\text{FeSe}_4$  tetrahedra and separated from each other by an interlayer distance of  $\sim 2.58 \text{ \AA}$ . The  $\text{SmFeAsO}_{1-x}\text{F}_x$  superconductors adopt a similar packing geometry made of  $\text{AsFeAs}$  slabs of  $\sim 2.7 \text{ \AA}$  thickness interleaved with  $\text{Sm}(\text{F},\text{O})$  layers which are absent in  $\alpha\text{-FeSe}_{0.92}$ . The absence of the charge reservoir layers leads to a drastically reduced  $c$  lattice constant of  $\sim 5.5 \text{ \AA}$  for  $\alpha\text{-FeSe}_{0.92}$  (*cf.*  $c \approx 8.5 \text{ \AA}$  for  $\text{SmFeAsO}_{1-x}\text{F}_x$ ). The basal plane lattice constants of  $\alpha\text{-FeSe}_{0.92}$  are also somewhat smaller than those in  $\text{SmFeAsO}_{1-x}\text{F}_x$  reflecting the shorter Fe–Se bond lengths (2.38  $\text{\AA}$  vs. 2.40  $\text{\AA}$  for the Fe–As bond lengths).

Finally, it has been argued before for the iron oxypnictide superconductors that the geometry of the  $\text{AsFe}_4$  pyramidal units (Fig. 1) sensitively controls both the Fe near- and next-neighbour exchange interactions<sup>10</sup> and the width of the electronic conduction band.<sup>3,11</sup> As a result, the superconducting transition onset  $T_c$  of  $\text{REFeAsO}_{1-x}\text{F}_x$  increases as the Fe–As–Fe angles become progressively smaller and the rare earth series is traversed with the  $\text{RE}^{3+}$  ionic radius decreasing. At present, there is no information available on the electronic structure of the iron selenide superconductors and the corresponding influence of the local geometry on the conduction bandwidth. Nonetheless we note that for  $\alpha\text{-FeSe}_{1-x}$ , the two small Fe–Se–Fe angles at  $\sim 68^\circ$  (Fig. 1c) are comparable to those in  $\text{SmFeAsO}_{1-x}\text{F}_x$  ( $\sim 71^\circ$ ), while the larger Fe–Se–Fe angle of the  $\text{SeFe}_4$  pyramids at  $\sim 105^\circ$  is considerably smaller than those of the iron oxyarsenides ( $> 111^\circ$ ).

In conclusion, we have found that the  $\alpha\text{-FeSe}_{0.92}$  superconductor adopts at low temperatures an orthorhombic superstructure of the high-temperature tetragonal  $\text{PbO}$ -type structure. The structural transition at  $\sim 70 \text{ K}$  is evidenced in the electronic properties *via* a hump in the temperature dependence of the resistivity. Given the very large positive pressure coefficient of  $T_c$  ( $\sim 9 \text{ K GPa}^{-1}$ ) in this material, it will be intriguing to follow the structural behaviour and the response of the orthorhombic distortion as a function of applied external pressure.

We thank the ESRF and the ILL for synchrotron X-ray and neutron beamtime, respectively.

## Notes and references

- 1 Y. Kamihara, T. Watanabe, M. Hirano and H. Hosono, *J. Am. Chem. Soc.*, 2008, **130**, 3296; X. H. Chen, T. Wu, G. Wu, R. H. Liu, H. Chen and D. F. Fang, *Nature*, 2008, **453**, 761; R. H. Liu, G. Wu, T. Wu, D. F. Fang, H. Chen, S. Y. Li, K. Liu, Y. L. Xie, X. F. Wang, R. L. Yang, L. Ding, C. He, D. L. Feng and X. H. Chen, *Phys. Rev. Lett.*, 2008, **101**, 087001; Y. Takabayashi, M. T. McDonald, D. Papanikolaou, S. Margadonna, G. Wu, R. H. Liu, X. H. Chen and K. Prassides, *J. Am. Chem. Soc.*, 2008, **130**, 9242.
- 2 C. de la Cruz, Q. Huang, J. W. Lynn, J. Li, W. Ratcliff, J. L. Zarestky, H. A. Mook, G. F. Chen, J. L. Luo, N. L. Wang and P. Dai, *Nature*, 2008, **453**, 899; T. Nomura, S. W. Kim, Y. Kamihara, M. Hirano, P. V. Sushko, K. Kato, M. Takata, A. L. Shluger and H. Hosono, arXiv:0804.3569, 2008.
- 3 J. Zhao, Q. Huang, C. de la Cruz, S. Li, J. W. Lynn, Y. Chen, M. A. Green, G. F. Chen, G. Li, Z. Li, J. L. Luo, N. L. Wang and P. Dai, arXiv:0806.2528, 2008.
- 4 S. Margadonna, Y. Takabayashi, M. T. McDonald, M. Brunelli, G. Wu, R. H. Liu, X. H. Chen and K. Prassides, arXiv:0806.3962, 2008.
- 5 Z. A. Ren, G. C. Che, X. L. Dong, J. Yang, W. Lu, W. Yi, X. L. Shen, Z. C. Li, L. L. Sun, F. Zhou and Z. X. Zhao, *Europhys. Lett.*, 2008, **83**, 17002.
- 6 M. Rotter, M. Tegel, D. Johrendt, I. Schellenberg, W. Hermes and R. Pottgen, *Phys. Rev. B: Condens. Matter Mater. Phys.*, 2008, **78**, 020503.
- 7 M. J. Pitcher, D. R. Parker, P. Adamson, S. J. C. Herkelrath, A. T. Boothroyd, S. J. Clarke, arXiv:0807.2228, 2008; J. H. Tapp, Z. Tang, B. Lv, K. Sasmal, B. Lorenz, P. C. W. Chu and A. M. Guloy, *Phys. Rev. B: Condens. Matter Mater. Phys.*, 2008, **78**, 060505(R).
- 8 F.-C. Hsu, J.-Y. Luo, K.-W. Yeh, T.-K. Chen, T.-W. Huang, P. M. Wu, Y.-C. Lee, Y.-L. Huang, Y.-Y. Chu, D.-C. Yan and M.-K. Wu, arXiv:0807.2369, 2008.
- 9 Y. Mizuguchi, F. Tomioka, S. Tsuda, T. Yamaguchi and Y. Takano, arXiv:0807.4315.
- 10 T. Yildirim, *Phys. Rev. Lett.*, 2008, **101**, 057010.
- 11 T. M. McQueen, M. Regulacio, A. J. Williams, Q. Huang, J. W. Lynn, Y. S. Hor, D. V. West, M. A. Green and R. J. Cava, *Phys. Rev. B: Condens. Matter Mater. Phys.*, 2008, **78**, 024521.